Supporting Information

Agarose-Based Fluorescent Waveguide with Embedded Silica nanoparticle-Carbon Nanodot Hybrids for pH Sensing

Francesco Amato,[a] Marco César Prado Soares,[b,c] Thiago Destri Cabral,[b,c] Eric Fujiwara,[b] Cristiano Monteiro de Barros Cordeiro,[c] Alejandro Criado,[d] Maurizio Prato[a,d,e] * and Julio Roberto Bartoli[b,f] *

[a]*Department of Chemical and Pharmaceutical Sciences,* ***INSTM UdR Trieste****,* ***University of Trieste****, Via Licio Giorgieri 1, 34127 Trieste, Italy.*
[b]*Laboratory of Photonic Materials and Devices,* ***School of Mechanical Engineering****,* ***State University of Campinas****, Campinas, SP, Brazil 13083-860.*
[c]*Laboratory of Specialty Fibers and Photonic Materials,* ***"Gleb Wataghin" Institute of Physics****,* ***State University of Campinas****, Campinas, SP, Brazil 13083-859*
[d]***Center for Cooperative Research in Biomaterials*** *(CIC biomaGUNE),****Basque Research and Technology Alliance*** *(BRTA), Paseo de Miramón 182, 20014, Donostia San Sebastián (Spain).*
[e]***Basque Foundation for Science****, Ikerbasque, 48013 Bilbao, Spain.*
[f]*Laboratory of Dielectrics, Optical and Nanocomposites Materials, Department of Materials and Bioprocess Engineering,* ***School of Chemical Engineering****,* ***State University of Campinas****, Campinas, SP, Brazil 13083-852.*

Corresponding authors
* Email: bartoli@unicamp.br (J.R.B.)
prato@units.it (M.P.)

Contents

1. Visual Comparison between Particles

Fig. S1 compares the aspect (observed under naked eye and daylight) of the three nanoparticles.

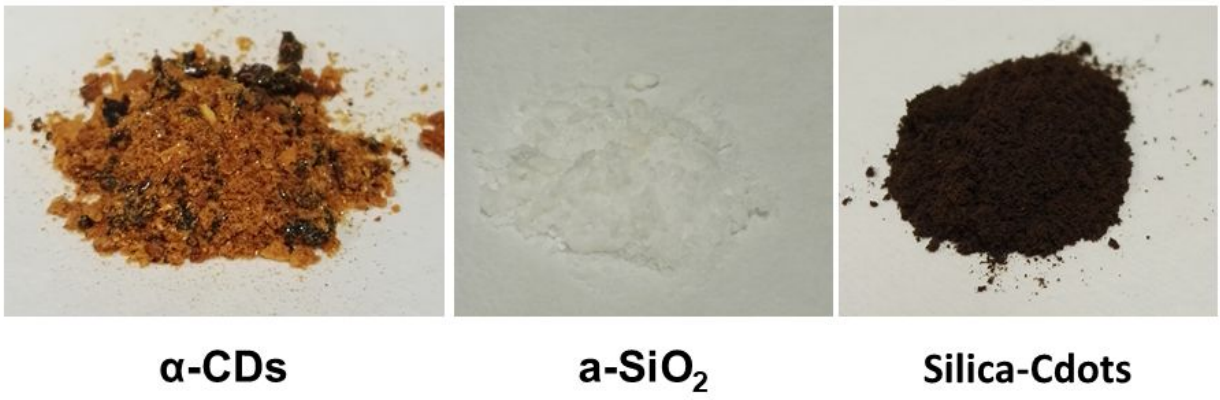

Figure S1. Different visual aspects observed for the nanoparticles.

2. Selection of the Light Source for the pH-Sensing Tests (403 nm-LED)

When selecting the light source for exciting the hybrid particles, there are 4 main factors that need to be considered: optical power, wavelength, cost, and safety. Taking into account these parameters, we have opted to use a 405 nm nominal wavelength (actual peak wavelength at 403 nm) high power (3 W) LED source with a full-width at half-maximum (FWHM, a measure of the broadness of the emission spectra) of 12 nm.

With this configuration, most of the optical power being emitted by the LED is in the 390-415 nm range. Moreover, about half of the optical power is in the visible range, providing more safety when handling a relatively high-powered UV source. The bulk of the emission spectrum of the LED is in a range that produce a good fluorescent response (as noticed on Fig. 3), with a strong response around the 390 nm range. The high maximum power (up to 3 W), in its turn, ensures that a strong response is observed even when not using a narrowband laser source near the peak excitation wavelength.

Finally, the LED used on the reported experiments had an approximate cost of 20 USD, while a narrowband laser would increase the cost by at least 1 to 2 orders of magnitude. Since our sensor was designed for being used in daily laboratory situations, the selection of this source allows the user to perform experiments without the necessity of elevated investments in both a specific source and in the high-performance UV-protection safe glasses necessary to handle it.

3. Numerical Aperture (NA) Evaluation

The Numerical Aperture (NA) may be understood as an indication of the efficiency in guiding light. It may be calculated using Equation S1, where n_{air} = 1.0000 is the refractive index of the air, considered the cladding of the waveguide (since no coating procedure was performed), and $n_{hydrogel}$ = 1.3334 is the refractive index of the doped hydrogel (considered the core).

$$NA \cong \sqrt{{n_{hydrogel}}^2 - {n_{air}}^2} \quad (S1)$$

It results in NA = 0.882, which is fairly high, indicating that the doped waveguide has an elevated capacity of capturing and guiding the luminescence radiation from the CD-doped hydrogel.

If the waveguide is supposed to be used immersed in water, than we may substitute n_{air} to n_{water} = 1.3330 in Equation S1. It leads to NA = 0.054, a value that is substantially lower, but still shows the guidance of light.

4. α-CDs UV-Visible Absorbance

UV-Visible (UV-Vis) absorbance analyses of aqueous suspensions of α-CDs in NaOH 0.1M, and of silica-Cdots in NaOH 0.1M were performed at room temperature with a Cary Ellipse-Varian Fluorescence Spectrophotometer (Agilent Technologies).

Both absorption spectra (Fig. S2) show maximum absorbance at 300 nm (which corresponds to the $\pi \rightarrow \pi^*$ transition of the sp^2 carbons of the CDs' cores), and a shoulder at 360 - 390 nm with a tail extending to the visible range. These shoulder and tail are assigned to the $n \rightarrow \pi^*$ transitions involving the electron lone pairs of the carboxylic surface groups.

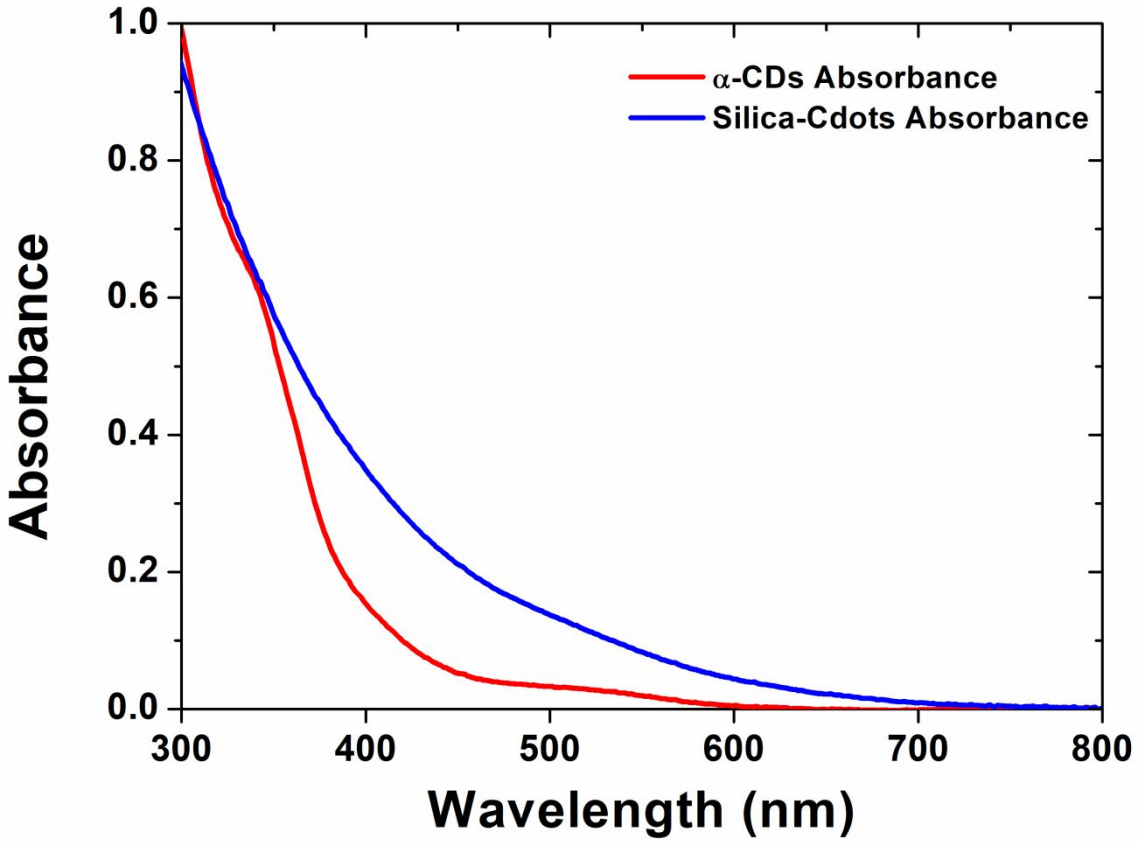

Figure S2. UV-Vis absorption spectra from α-CDs (in red) and from silica-Cdots (blue).

5. TEM and FEG-TEM Images of Particles

Fig. S3 shows TEM and FEG-TEM images of α-CDs. Fig. S4 and S5 show TEM images of a-SiO_2 and silica-Cdots nanoparticles, respectively. Once the particles are amorphous, they are hardly observed. Despite this intrinsic difficulty for the analysis, the variation of diameter and morphology is clearly noticed.

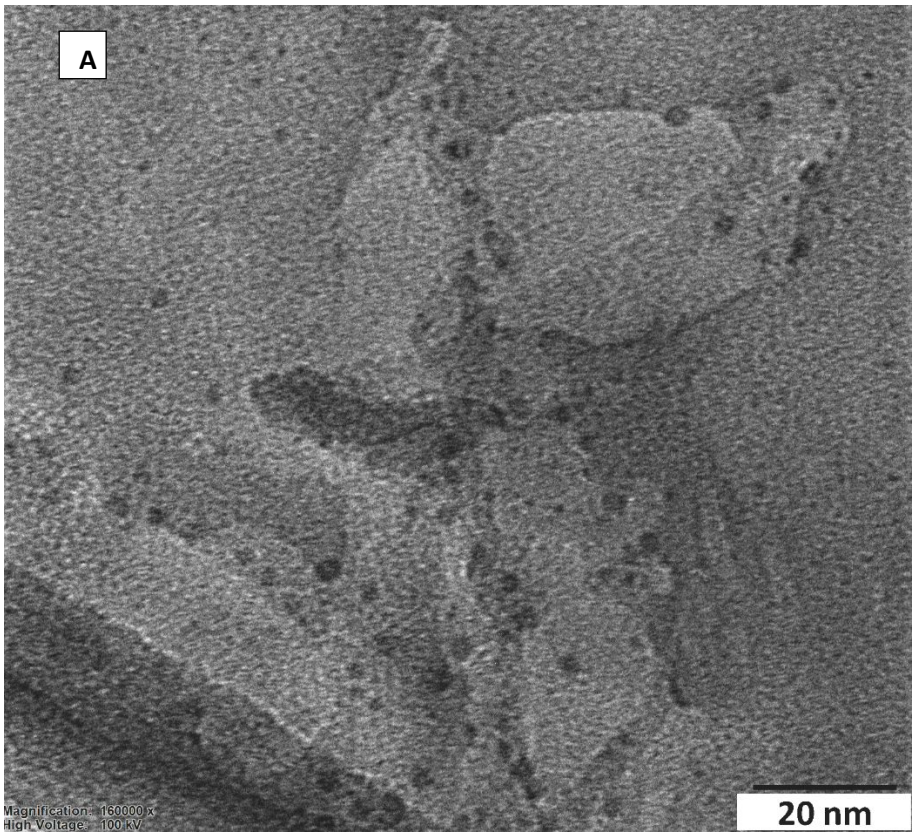

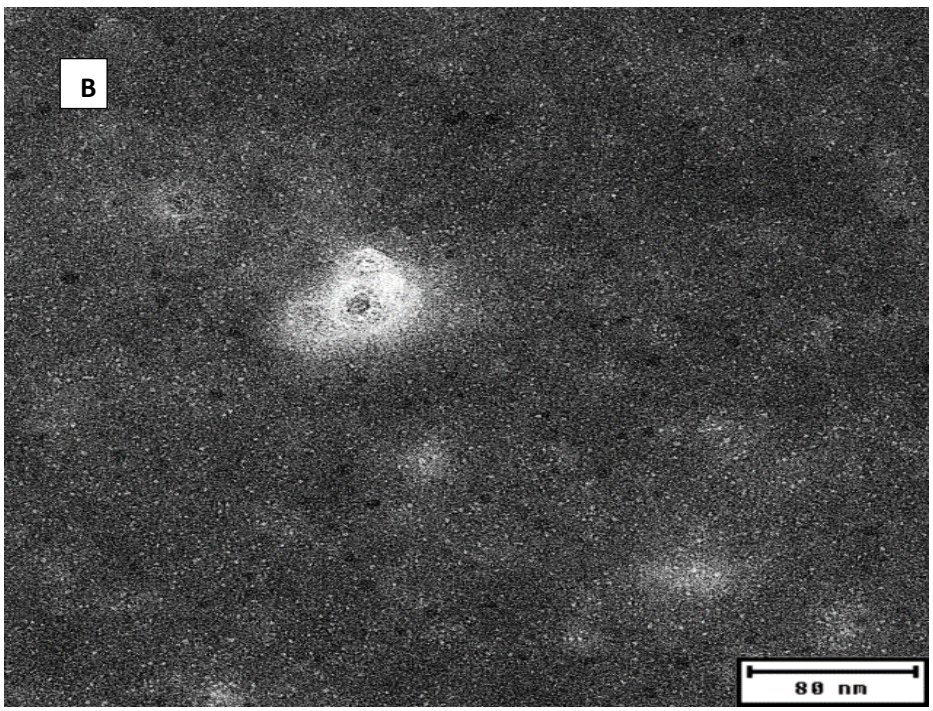

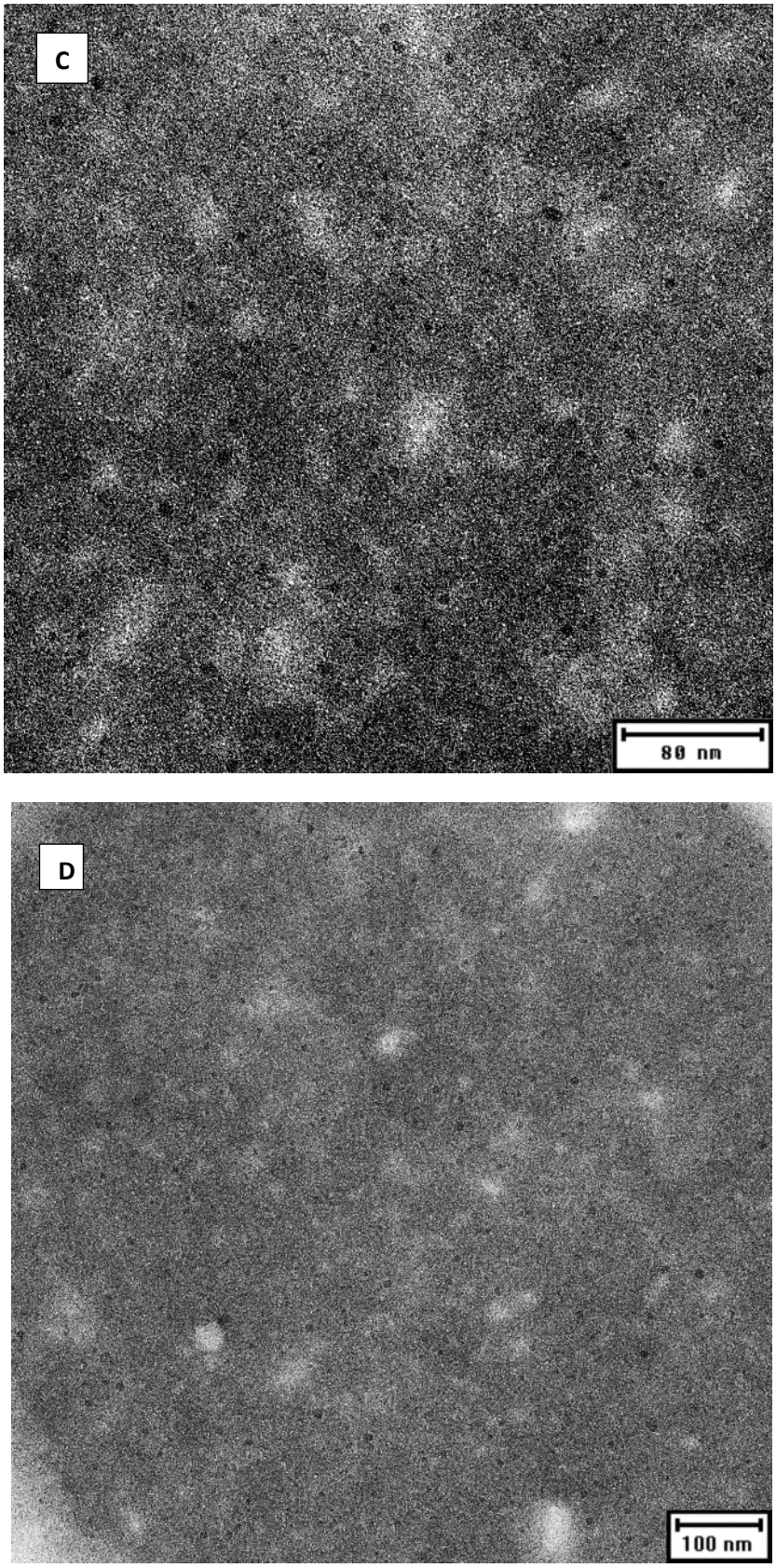

Figure S3: Micrographs of α-CD primary nanoparticles, sizes between ~4 nm and ~10 nm: (A) TEM image; (B), (C) and (D) negative stained FEG-TEM images (color inverted to facilitate viewing).

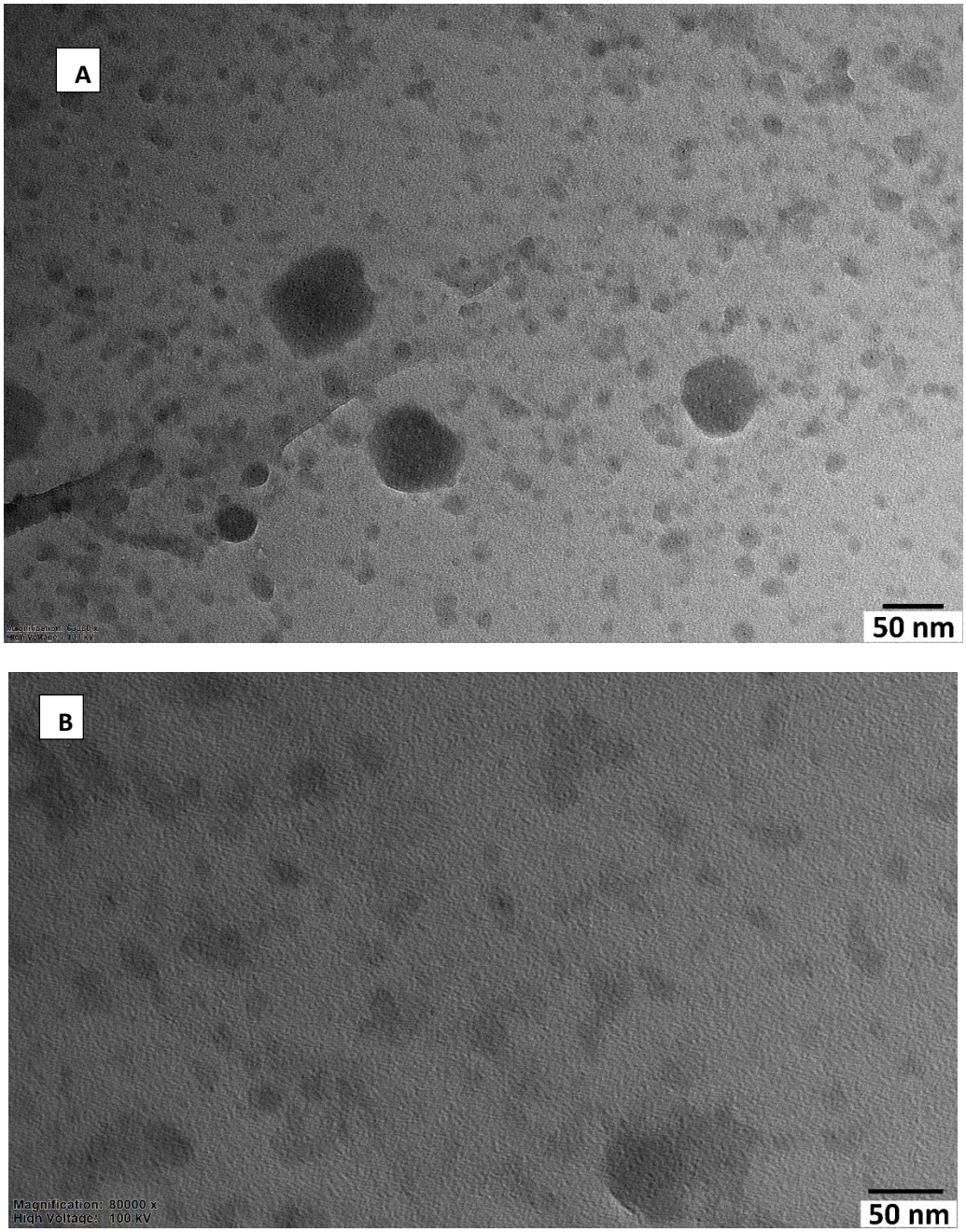

Figure S4. TEM images of a-SiO_2 aggregates and primary particles;
(magnification: (A) 63 x 10^3 times, (B) 80 x 10^3 times).

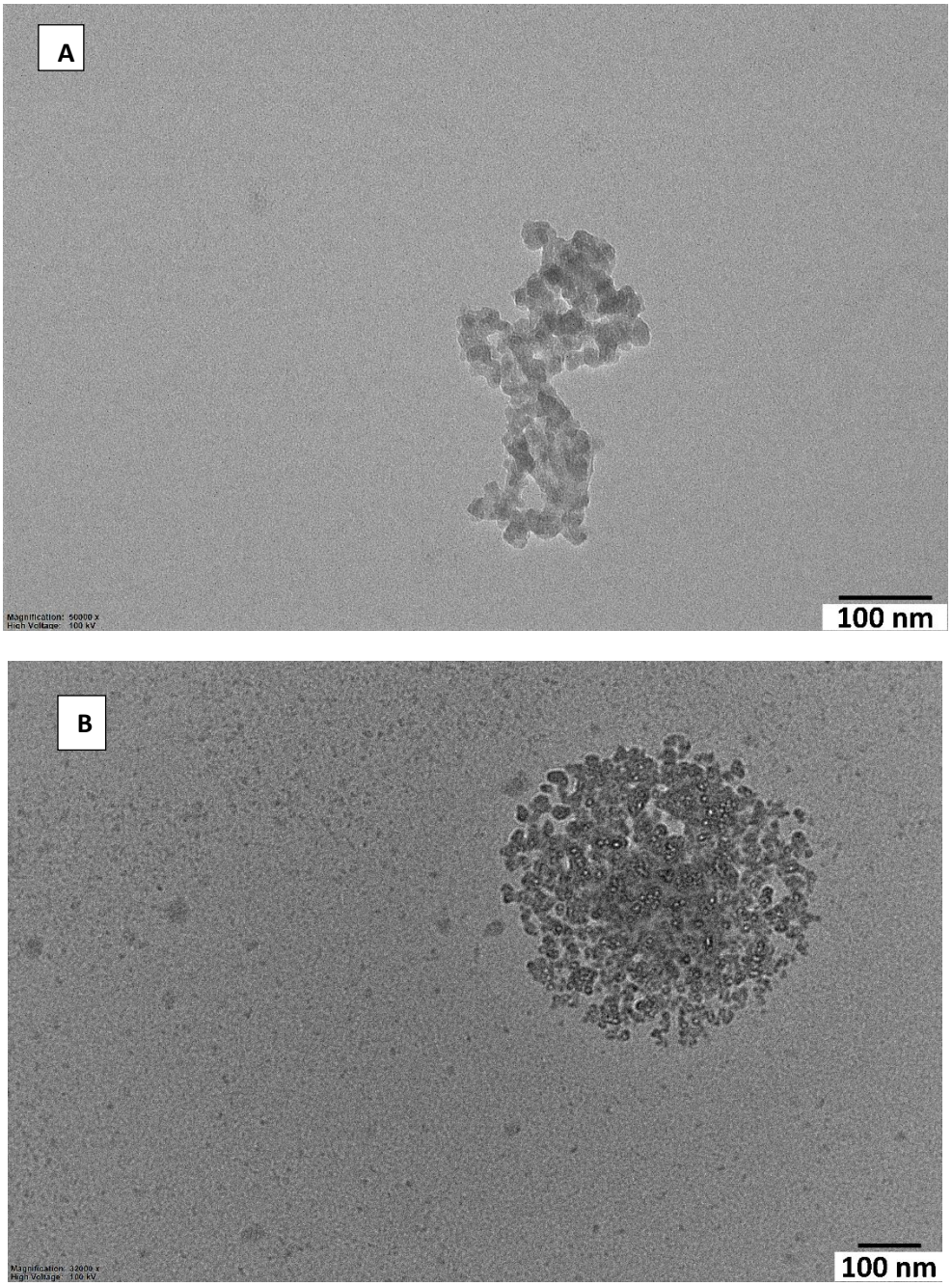

Figure S5. TEM images of silica-Cdots aggregates and primary particles (magnification: (A) 50 x 10^3 times, (B) 32 x 10^3 times).

6. Comparison between FT-IR Spectra of the Particles

Fig. S6, S7 and S8 show the SiO_2, a-SiO_2, α-CDs and silica-Cdots nanoparticles FT-IR spectra compared by pairs. All the peaks and bands are indexed to demonstrate the formation of the chemical bonds after the amino-functionalization of the SiO_2 and the coupling reaction with α-CDs

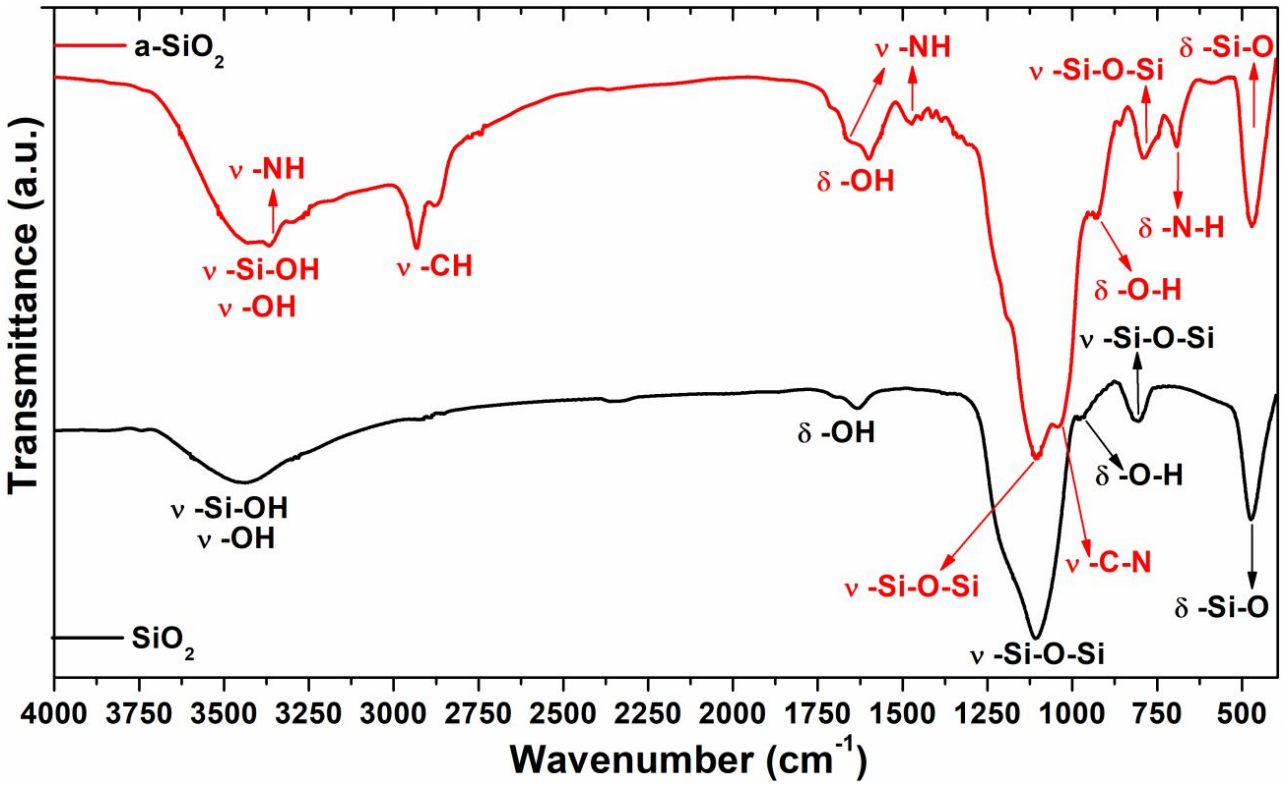

Figure S6. Comparison between FT-IR spectra of SiO_2 and a-SiO_2.

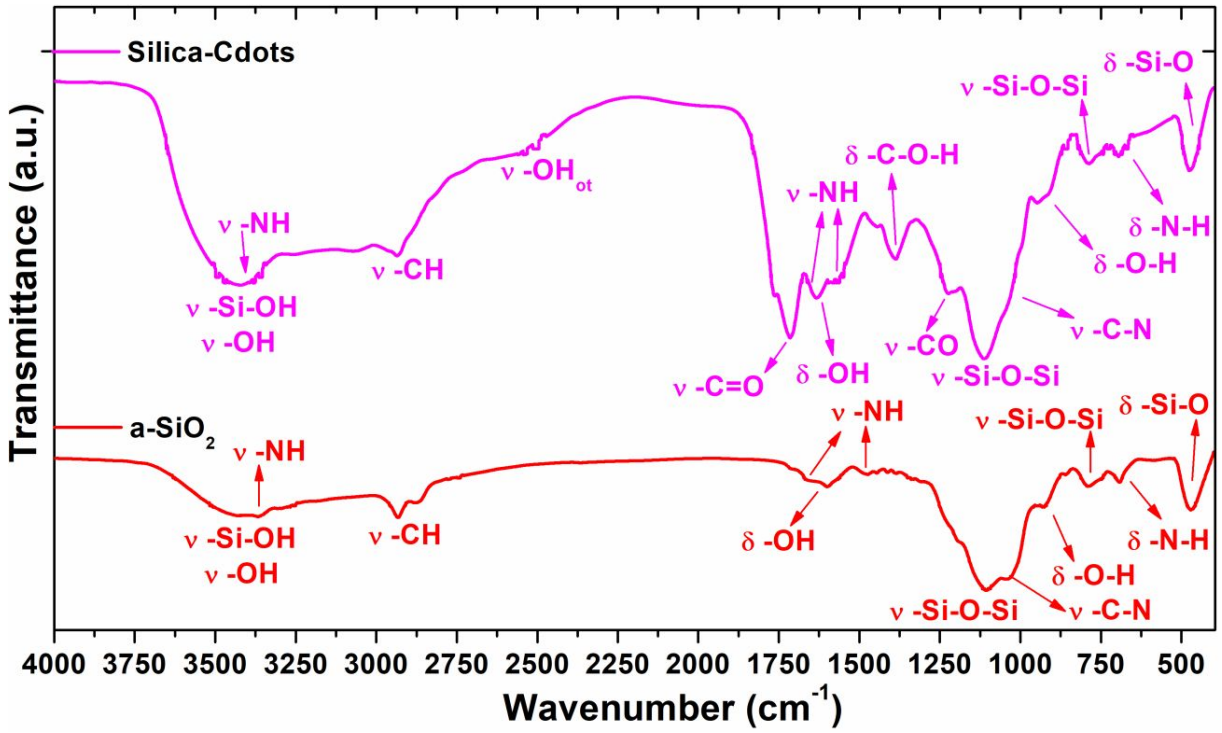

Figure S7. Comparison between FT-IR spectra of a-SiO_2 and silica-Cdots.

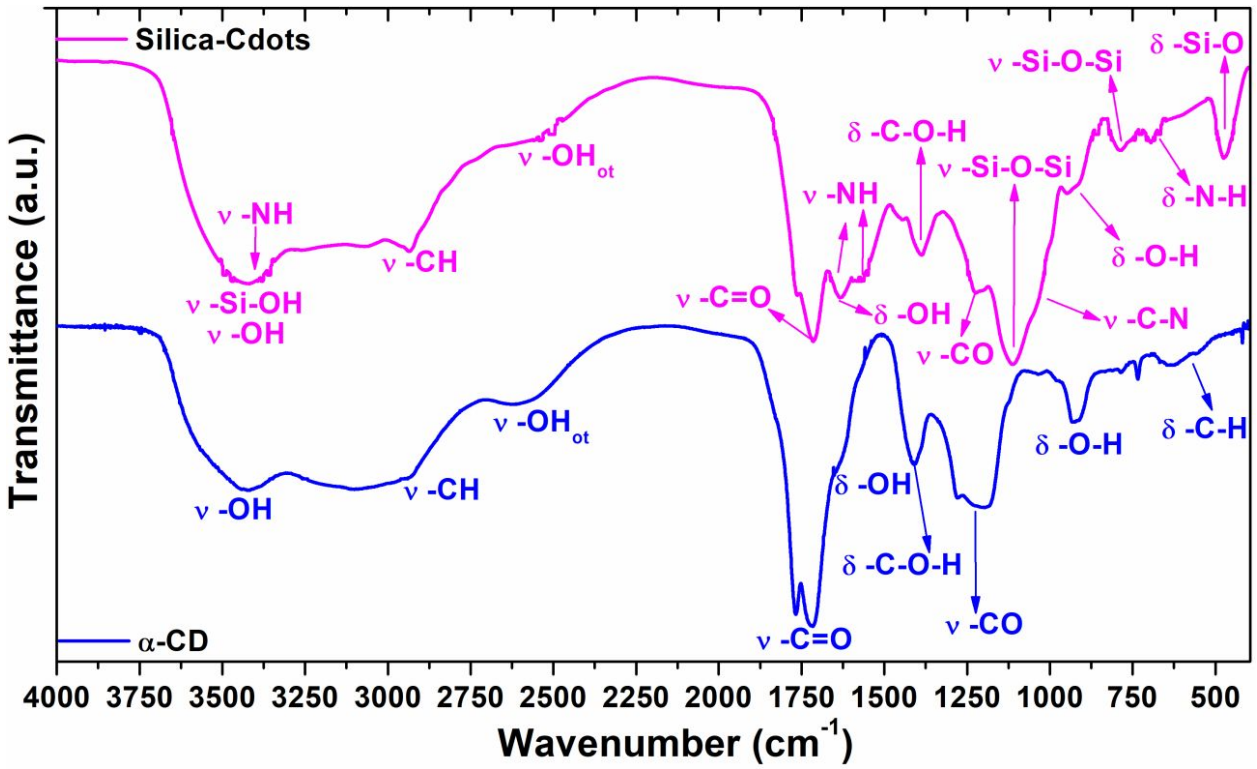

Figure S8. Comparison between FT-IR spectra of α-CDs and silica-Cdots.

7. Thermogravimetric Analysis (TGA) of the Particles

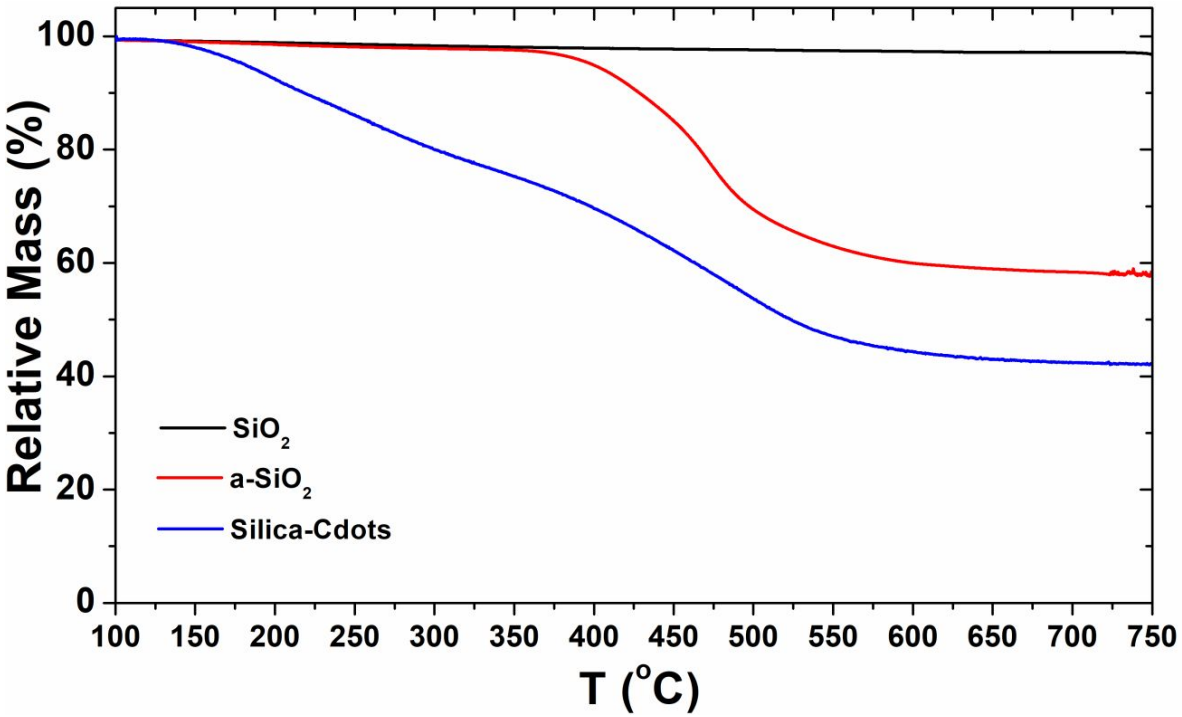

Figure S9. TGA of nanoparticles of fumed silica, amino-functionalized silica, and silica-Cdots hybrid.

8. XPS Analyses of the Particles

Fig. S10, S11 and S12 show the high-resolution XPS spectra for the core-level C 1s, N 1s, O 1s and Si 2p peaks of the a-SiO_2, α-CDs and silica-Cdots nanoparticles. The individual contributions of different functional groups present in the materials are shown.

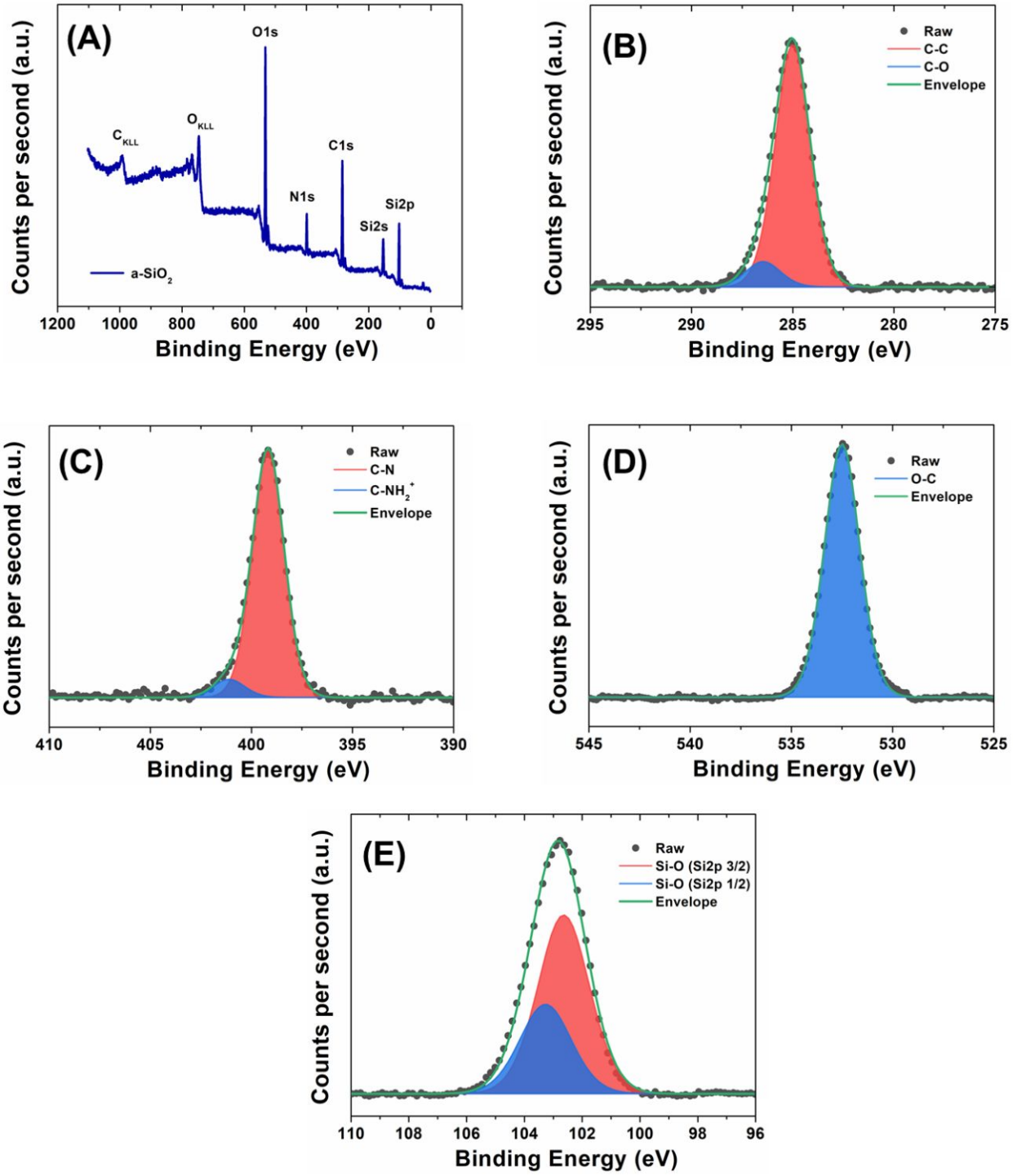

Figure S10. (A) XPS spectrum for a-SiO_2; and XPS high resolution spectra: (B) C1s; (C) N1s; (D) O1s; (E) Si2p obtained for a-SiO_2.

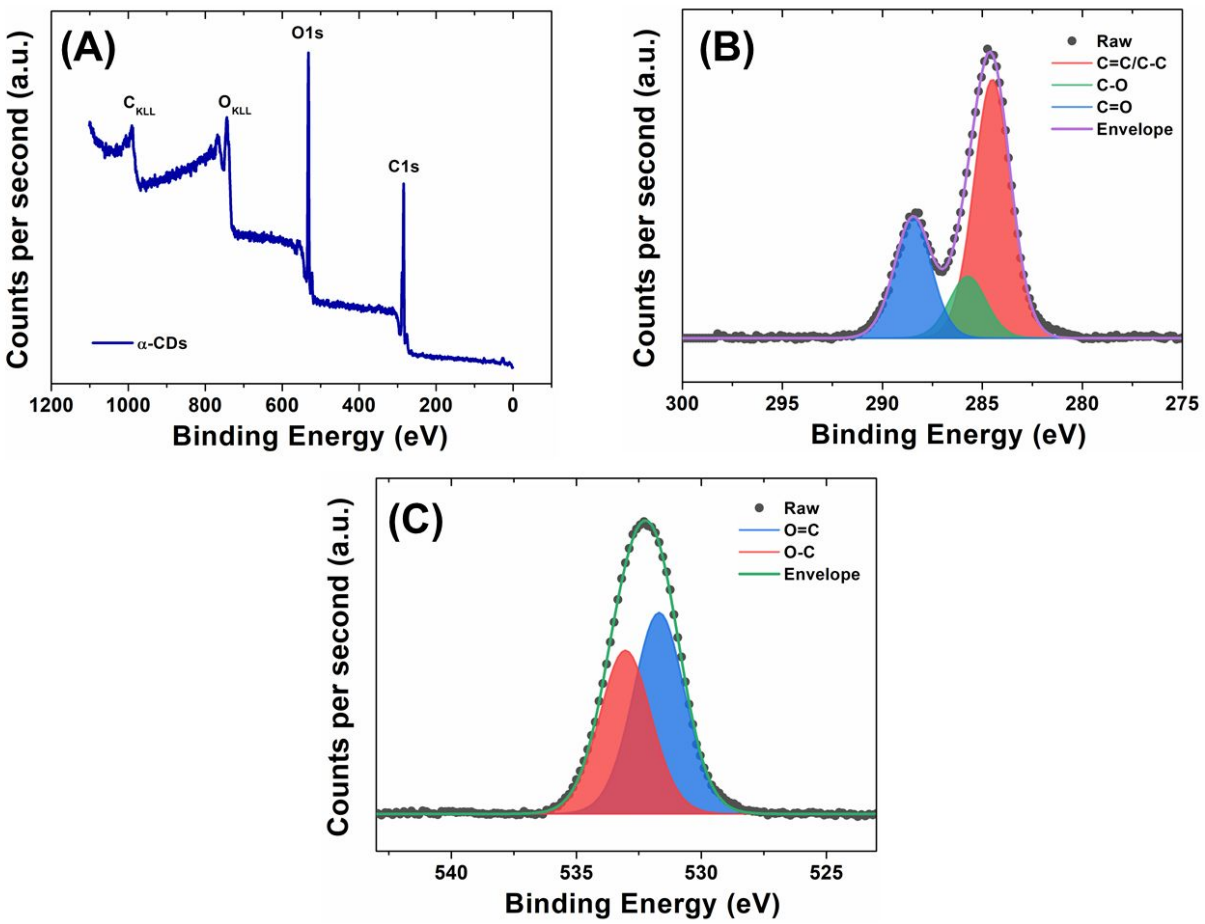

Figure S11. (A) XPS spectrum for α-CDs; and XPS high resolution spectra: (B) C1s; (C) O1s obtained for α-CDs.

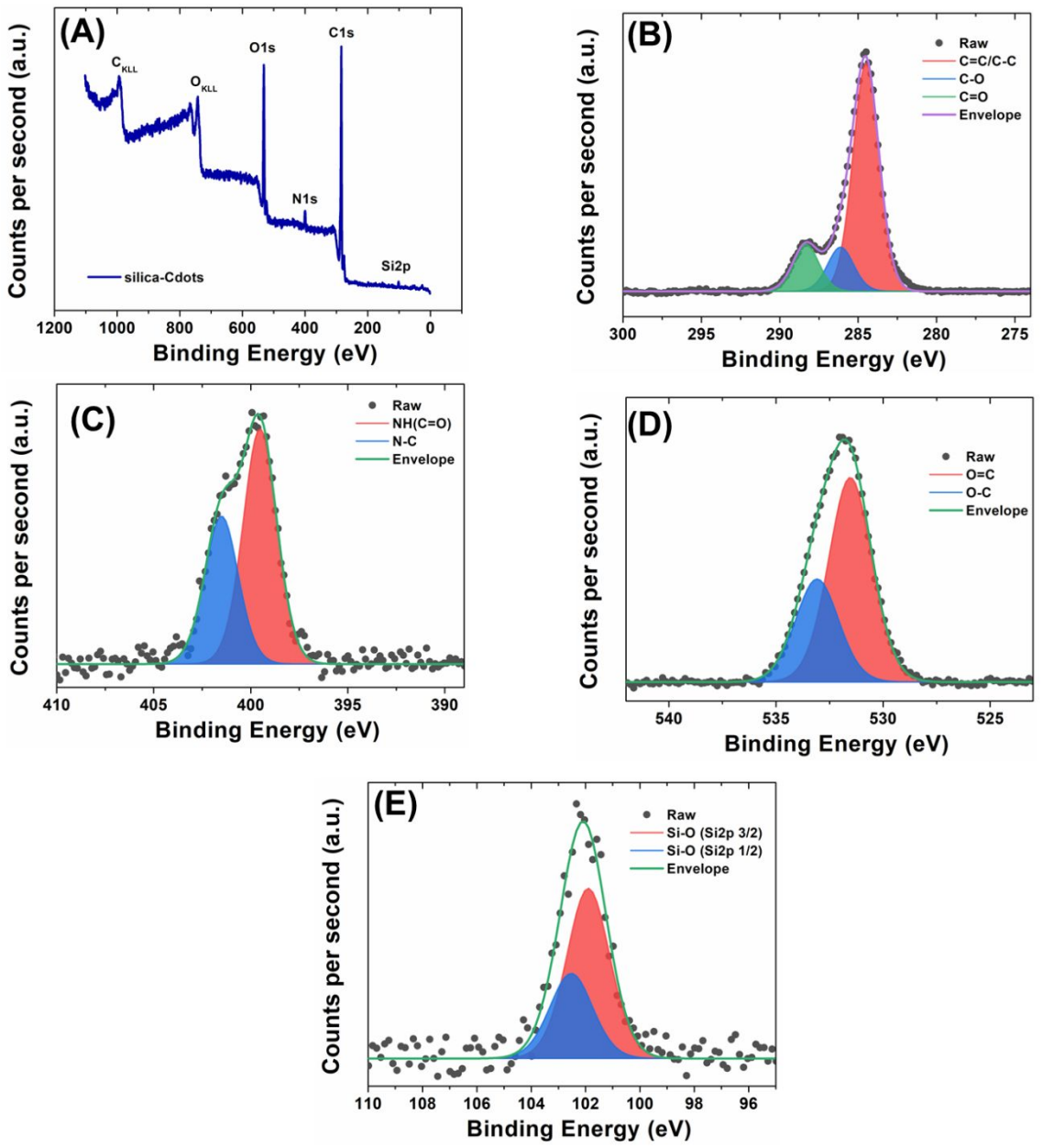

Figure S12. (A) XPS spectrum for silica-Cdots; and XPS high resolution spectra: (B) C1s; (C) N1s; (D) O1s; (E) Si2p obtained for silica-Cdots.

Table S1. Atomic percentages of samples obtained by high-resolution XPS spectra

Sample	C / at%	O / at%	N / at%	Si / at%
α-CDs	68.1	31.9	-	-
a-SiO_2	39.3	27.3	8.2	25.3
silica-Cdots	74.3	19.9	4.3	1.5

9. XRD Analyses of the Particles

Fig. S13 shows the XRD spectra of the SiO_2, a-SiO_2, α-CDs and silica-Cdots nanoparticles. The amorphous characteristics of all the nanoparticles were confirmed, as only amorphous halos and no XRD reflections typical of crystalline structures were observed, as follow:

SiO_2: the amorphous halo of the fumed SiO_2 is observed at around 2θ = 21.5°.

α-CD: the amorphous halo observed around 2θ = 18.5° could be due to some oxidized graphitic species; in turn the presence of graphitic species is imperceptible, as only a very smooth tail is observed around 2θ = 30°. Diffraction patterns for graphite and oxidized graphite are expected with strong reflections at 27º and 16º, respectively.

a-SiO_2: two amorphous halos are observed around 2θ = 8.5° and 2θ = 21.5° due to the amino group and SiO_2, respectively.

silica-Cdots: the amorphous halo of SiO_2 (~ 21.5°) overlaps the α-CD halo (shoulder at ~ 18.5°) and some contribution of the amino group is observed (~ 8.5°).

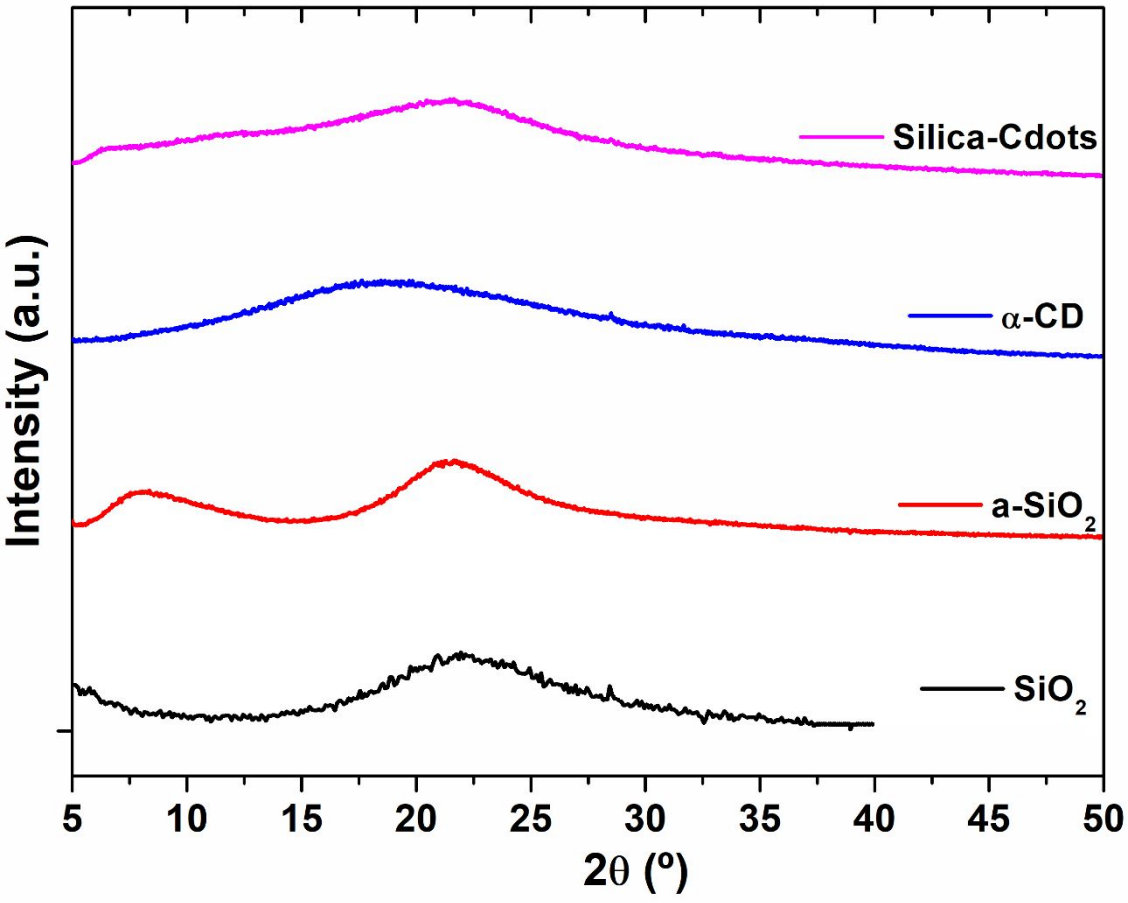

Figure S13: XRD patterns of the SiO_2, a-SiO_2, α-CDs and silica-Cdots nanoparticles.

10. Raman Spectra of the Particles

Figure S14 shows the Raman spectra (532 nm laser line) of α-CDs and silica-Cdots nanoparticles. No scattering signal and only fluorescence was observed in the hybrids and carbon nanodots.

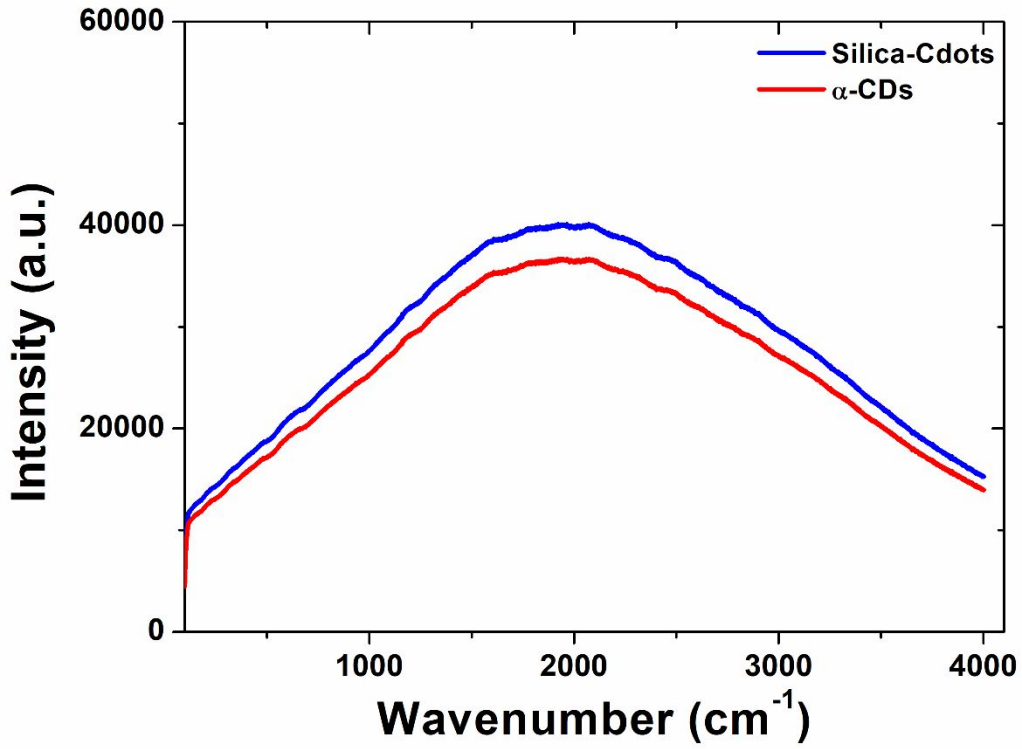

Figure S14: Raman spectra (@ 532 nm) of the α-CDs and silica-Cdots nanoparticles.

11. Setup for pH Evaluation in Aqueous Phase

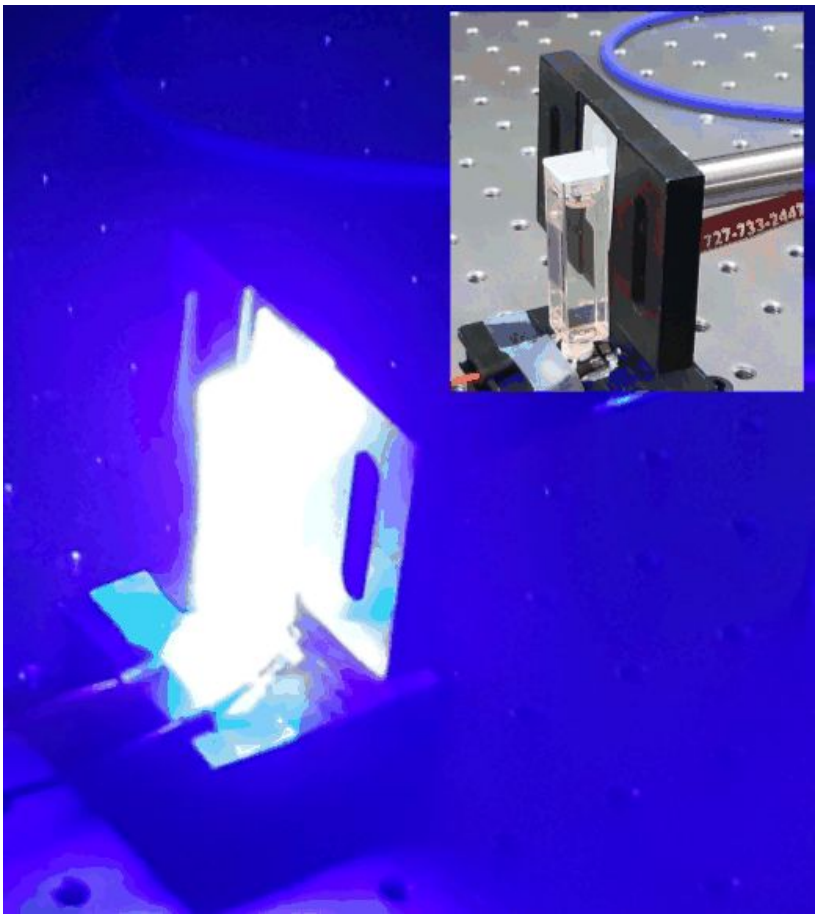

Figure S15. Assembled system with aqueous dispersions of silica-Cdots under UV-excitation, and under daylight (inset).

12. Emission Spectrum of the Light Source (Supercontinuum Laser)

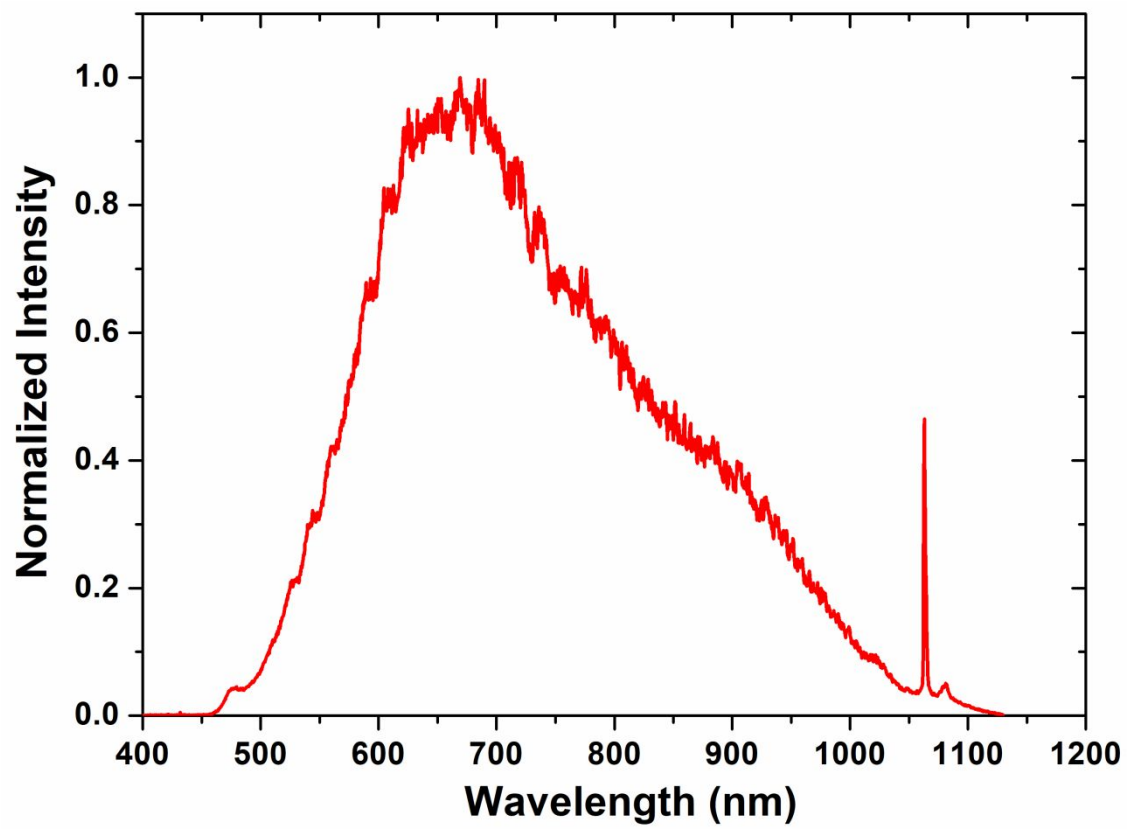

Figure S16. Emission Spectrum of the Light Source.

13. Agar and Silica-Cdots Doped Waveguides under Daylight and Supercontinuum

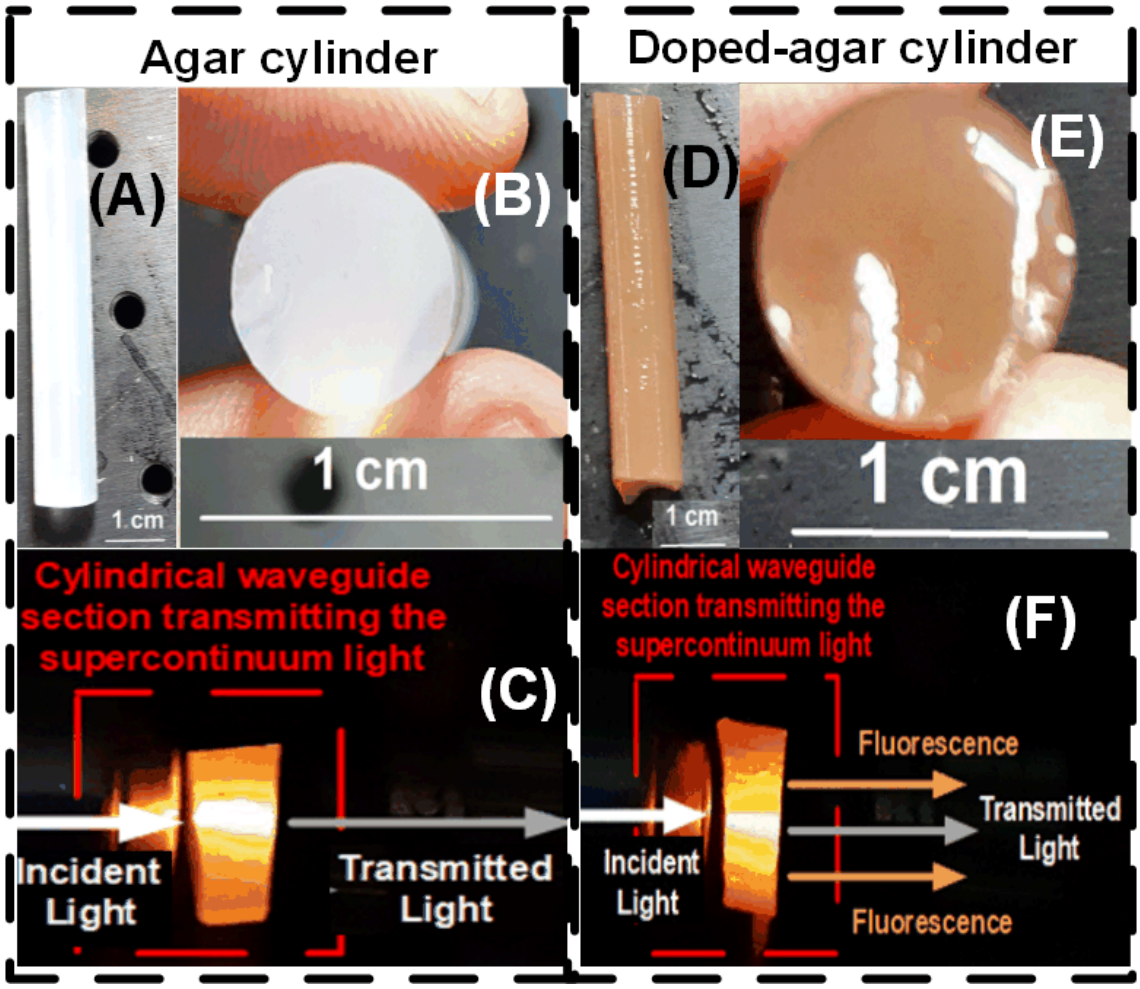

Figure S17. (A) General aspect of the agar waveguide; (B) cross-section of the agar waveguide; (C) agar waveguide transmitting the supercontinuum laser; (D) general aspect of the waveguide with occluded silica-Cdots hybrids; (E) cross-section of the waveguide with occluded hybrids; and (F) waveguide with occluded hybrids transmitting the supercontinuum laser.

14. Refractive Index (RI) of the Waveguide as Function of the Agar Concentration

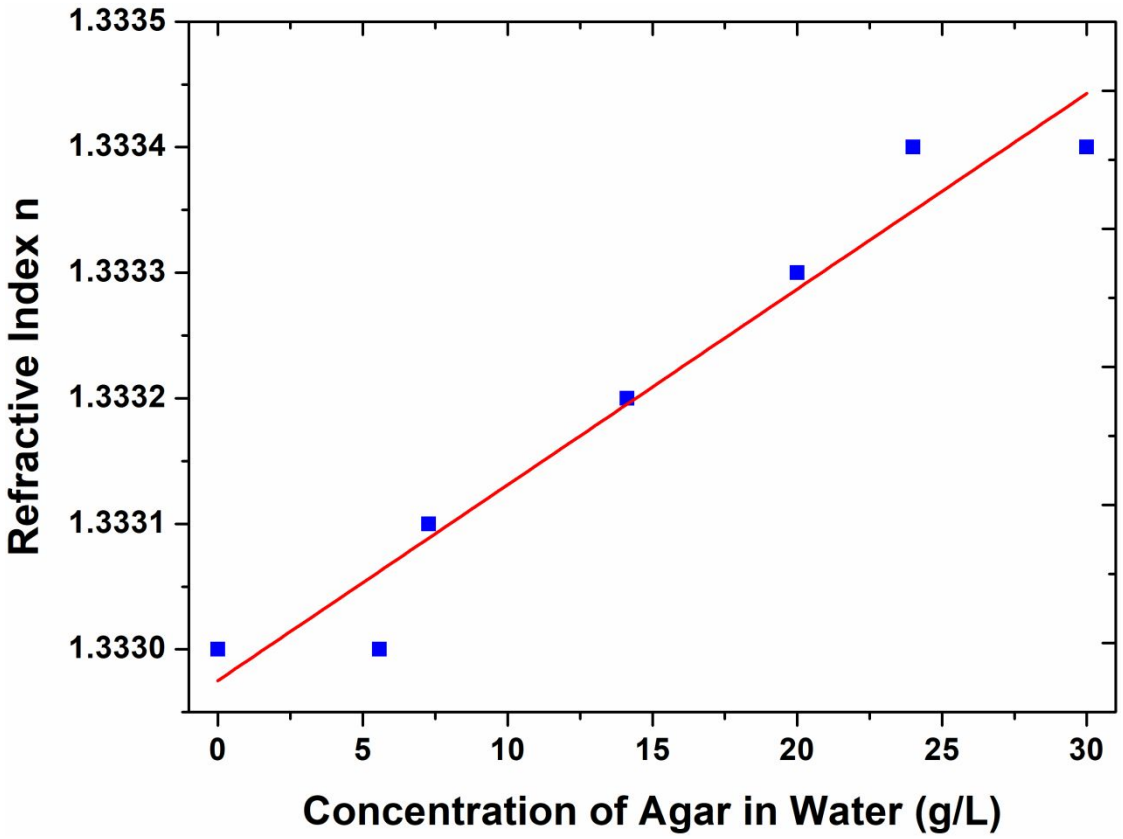

Figure S18. Refractive index of the waveguide as function of the agar concentration in the liquid precursor. The variation is in the order of only 10^{-4} refractive index units (RIU).

Additions of agar beyond 30 g/L were also tested, but the opacity of the final materials progressively grown. It led to significant increases of the light attenuation. On the other hand, the use of higher concentrations of agar resulted in very low variations of the mother liquor's refractive index, always in the order of only 10^{-4} refractive index units (RIU).

In fact, the RI variation associated with the curing process showed to be more significant than the one associated with the increase of the agar concentration in the precursor solution. Therefore, the chosen condition should be the one that resulted in the best combination of light transmittance and mechanical properties.

We verified that the best combination was obtained when using the concentration of 30 g/L. Thus, this value was selected for the waveguides fabrication, resulting in refractive indices of 1.3334. This value is still very close to the water's (1.3330).

15. Emission Spectra of Silica-Cdots under 403 nm and pH 4.30 (Water and Agar)

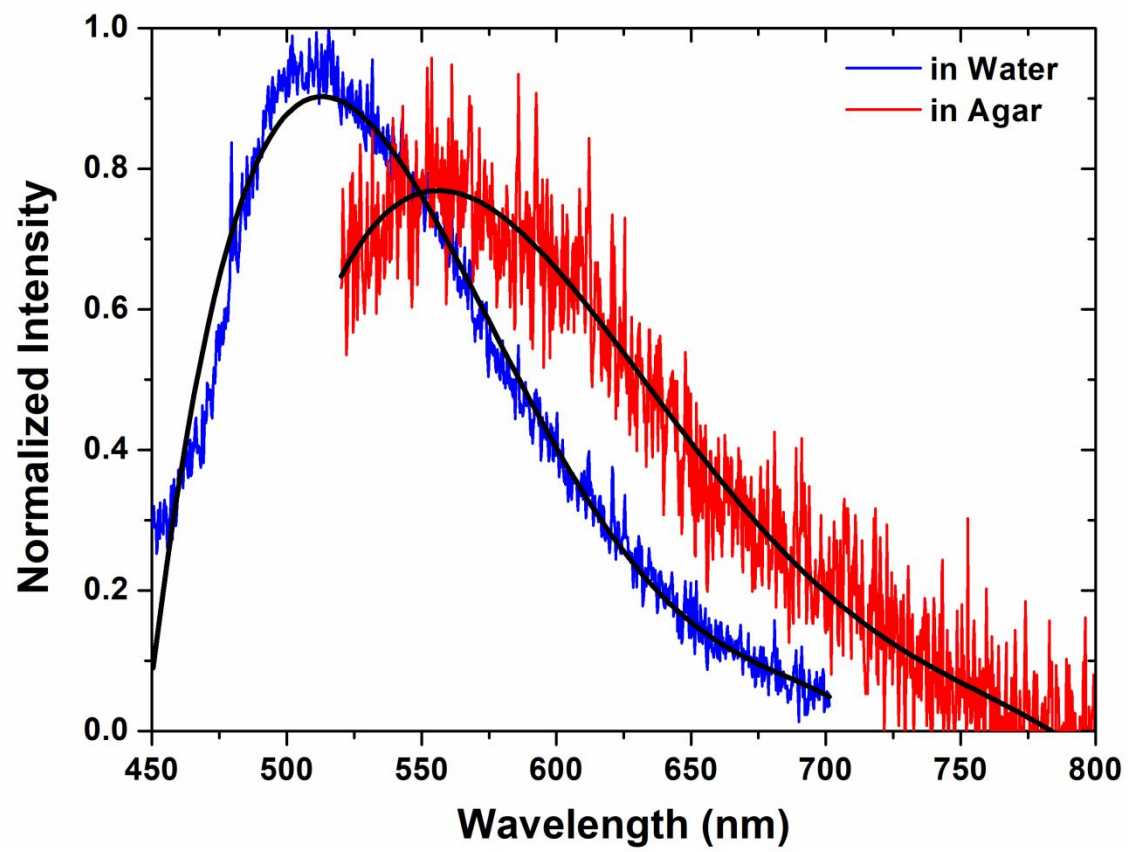

Figure S19. Fluorescence spectra of the silica-Cdots hybrids at excitation wavelength of 403 nm (when dispersed in water and when occluded into the agarose matrix) for pH 4.3, exhibiting the corresponding red-shift wavelength.